URANIUM METAL POWDER PRODUCTION, PARTICLE DISTRIBUTION ANALYSIS, AND REACTION RATE STUDIES OF A HYDRIDE-DEHYDRIDE PROCESS

An Honors Fellows Thesis

by

WILLIAM JAMES SAMES V

Submitted to the Honors Programs Office
Texas A&M University
in partial fulfillment of the requirements for the designation as

HONORS UNDERGRADUATE RESEARCH FELLOW

April 2011

Major: Nuclear Engineering

URANIUM METAL POWDER PRODUCTION, PARTICLE DISTRIBUTION ANALYSIS, AND REACTION RATE STUDIES OF A HYDRIDE-DEHYDRIDE PROCESS

An Honors Fellows Thesis

by

WILLIAM JAMES SAMES V

Submitted to the Honors Programs Office
Texas A&M University
in partial fulfillment of the requirements for the designation as

HONORS UNDERGRADUATE RESEARCH FELLOW

Approved by:

Research Advisor: Sean M. McDeavitt
Associate Director of the Honors Programs Office: Dave A. Louis

April 2011

Major: Nuclear Engineering

ABSTRACT

Uranium Metal Powder Production, Particle Distribution Analysis, and Reaction Rate Studies of a Hydride-Dehydride Process. (April 2011)

William James Sames V
Department of Nuclear Engineering
Texas A&M University

Research Advisor: Dr. Sean McDeavitt
Department of Nuclear Engineering

Work was done to study a hydride-dehydride method for producing uranium metal powder. Particle distribution analysis was conducted using digital microscopy and grayscale image analysis software. The particle size was found to be predominantly in the 40 μm range, which agreed with previous work. The effects of temperature, pressure, and time on the reaction fraction of powder were measured by taking experimental data. The optimum hydride temperature for the system was found to be 233.4°C. Higher gas pressures resulted in higher reaction fractions, over the range studied. For the sample parameters studied, a time of 371 minutes was calculated to achieve complete powderization. System design parameters for commercialization are proposed.

DEDICATION

This work is dedicated my parents for their unending support of everything that I do.

ACKNOWLEDGMENTS

I would like to thank my parents, family, friends, and teachers for their support of my pursuit of an education.

I would like to thank Dr. Sean McDeavitt for his support and guidance in this research.

I would like to thank all the students in the Fuel Cycles and Materials Laboratory for help, advice, and camaraderie along the way.

I would like to thank David Garnetti for his work in developing the hydride-dehydride system used in this research.

I would like to thank Grant Helmreich for his work in particle analysis, nitric acid chemistry, and teaching me about the hydride-dehydride process.

I would also like to thank Dr. D. Cecala and the Y-12 plant in Oak Ridge, Tennessee for providing the depleted uranium used in this project.

NOMENCLATURE

α	Reaction Fraction
ACV	Atmosphere Containment Vessel
AFCI	Advanced Fuel Cycle Initiative
FCML	Fuel Cycle and Materials Laboratory
GC	Growth Center
H_2	Hydrogen Gas
NERI	Nuclear Energy Research Initiative
ORNL	Oak Ridge National Laboratory
P	Pressure
T	Temperature
t	Time
TRU	Transuranic
U	Uranium
UH_3	Uranium-Hydride

TABLE OF CONTENTS

CHAPTER Page

LIST OF FIGURES

FIGURE Page

CHAPTER I

INTRODUCTION AND BACKGROUND

Different forms of nuclear fuel are used in different reactor designs. One fuel type, metal fuel, is of particular interest for fast reactor systems. These fuels frequently involve varying compositions of Uranium, Plutonium, and Zirconium (U-Pu-Zr). Transuranic (TRU) wastes are produced during the use of nuclear fuel. These waste products can be transmuted, or eliminated, by incorporation in fast reactor fuel in a Uranium-Transuranic-Zirconium (U-TRU-Zr) fuel. Powder metallurgy and injection casting are current methods of manufacturing metal fuels. Powder metallurgy requires metal powders that are pressed and sintered into fuel pellets. Powder metallurgy of uranium metal is under investigation at Texas A&M University for its potential to solve problems of transuranic volatility in U-TRU-Zr fuel manufacture. The production of uranium powder from larger pieces of uranium is necessary to make this process work. One method of powderizing uranium metal is to hydride the metal at elevated temperatures and then dehydride the hydride powder to produce uranium metal powder. This powder can then be blended with other metal or transuranic powders to create the desired composition for a fast reactor fuel pellet.

This thesis follows the style of Journal of Nuclear Materials.

Description of hydride

Uranium metal (U) forms uranium-hydride (UH_3) when subjected to temperatures greater than 150°C and hydrogen gas (H_2). [1] The temperature dependence of the reaction is shown in Figure 1 at constant pressure. The peak H_2 consumption corresponds to the peak reaction temperature at ~225°C. [2] This reversible reaction proceeds according to Eq. 1.

$$U + \frac{3}{2}H_2 \leftrightarrows UH_3 \quad (1)$$

The uranium metal usually has a thin oxide (UO_2) layer present on the surface. This oxide layer can be between 10-100 nm thick and still allow for the progression of the hydride reaction. [3] Thicker oxide layers can impede or prevent the reaction. The H_2 diffuses through the oxide layer to react with the U surface. [4] The difference in the density of uranium (18.9 g/cc) and UH_3 (10.3 g/cc) facilitates the formation of powder. [5] The corresponding increase in volume can lead to the precipitation of UH_3 blisters as shown in Figure 2. [4, 5, 6]

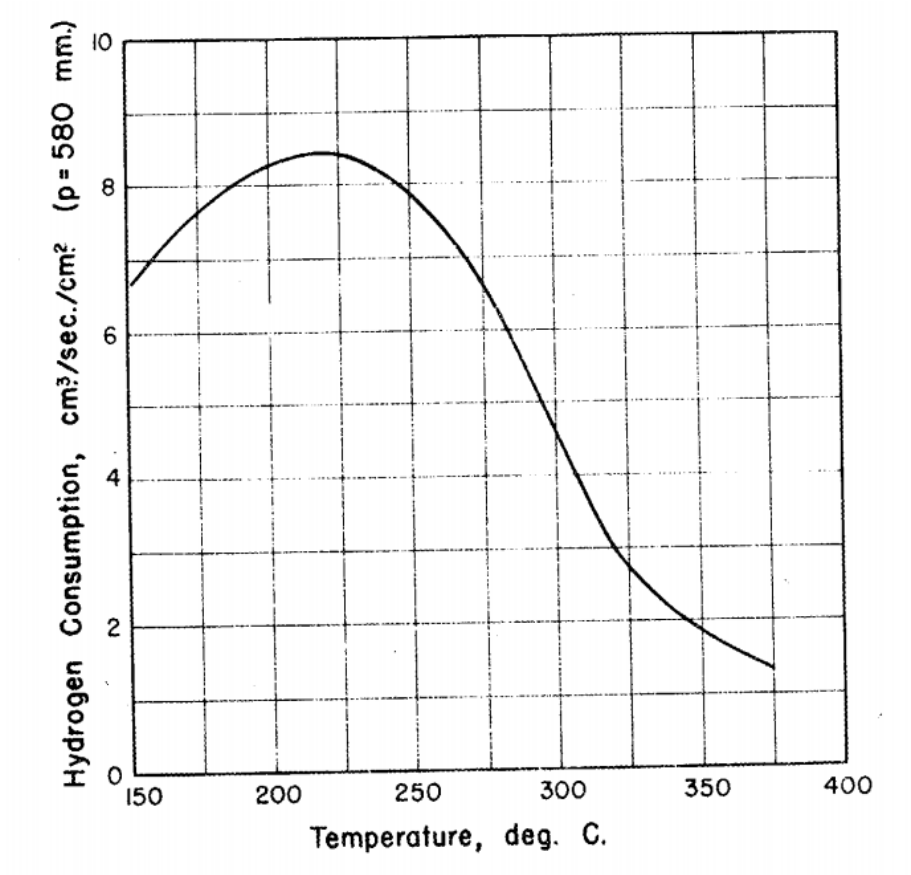

Figure 1. Temperature dependence of the hydride reaction. [2]

The hydrogen reacts at nucleation sites that are located beneath a small oxide layer as shown in Figure 2. Initial nucleation sites are small, on the order of a few nm. [3] Nucleation sites remain small, unless locate near a defect in the oxide layer. The growth of the blister near the defect can lead to the fracture of the oxide layer, and the continuance of the hydride reaction [3] A site at which this fracture occurs is described as a Growth Center (GC). [3] Approximately 77% of the nucleation sites were observed near grain or twin boundaries of the uranium metal by Bingert. [4] In the case of no oxide layer, nucleation occurs at the metal surface and continues unimpeded by an oxide

layer. As volume swelling breaks down the lattice structure, powder forms on the surface of the slug. Depending on the system, fluid or other motion can mechanically remove the powder layer, further exposing more uranium metal for reaction. It is also possible for continued hydrogen diffusion. If the powder layer sits on the uranium metal piece, the reaction rate will be impeded by the reduction in reactive surface area.

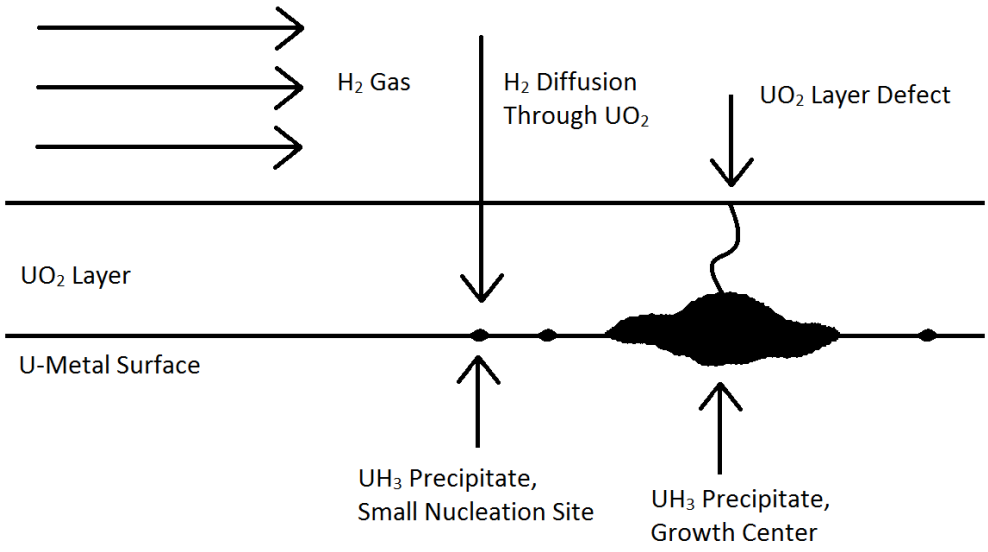

Figure 2. Sketch showing formation of UH_3 precipitate on a microscopic level.

Bingert's results show that hydrogen will diffuse through a layer of uranium dioxide (UO_2) on uranium metal to react and form uranium-hydride (UH_3). [4] The formation results in the formation of a "blister" at the metal-oxide interface. The blister formation is due to the change in volume associated with the formation of UH_3. An observation

made of this phenomenon is shown in Figure 3 (blister figure). The thickness of the UO_2 layer is proposed to be important to the formation of UH_3.

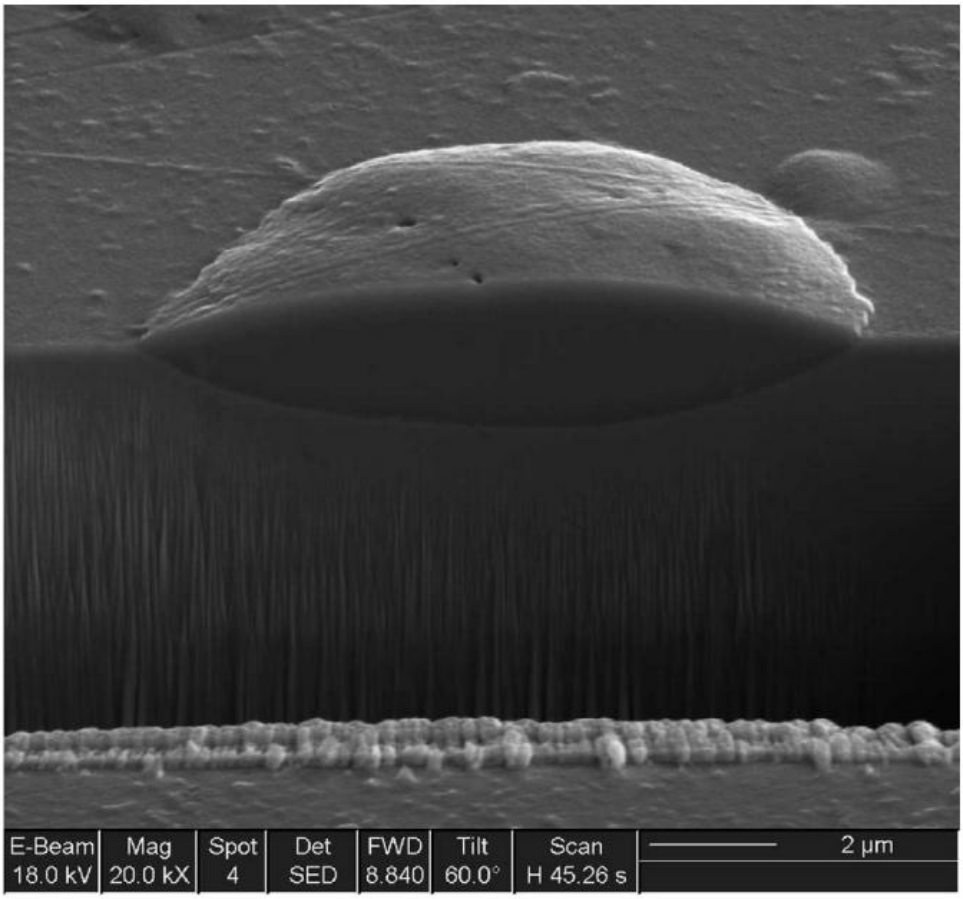

Figure 3. UH_3 blister formation at the oxide-metal interface. [4]

Description of dehydride

Uranium-hydride (UH_3) dissociates to uranium metal (U) and hydrogen gas (H_2) when subjected to temperatures above 430°C at atmospheric pressure. [2] The dissociation occurs at lower temperatures, for lower pressures. The relationship between temperature and pressure is exponential and is shown in Figure 4. The dehydride reaction is the reverse of the hydride reaction and proceeds according to Eq. 1 as well.

Starting with uranium-hydride powder, the reaction leaves behind uranium metal powder. Work by Garnetti shown in Figure 5 shows a rise in the pressure of a reaction vessel system under vacuum from the dehydride process. The rise in pressure is associated with the release of hydrogen gas from the UH_3 powder. This reaction was shown to usually complete within 20 minutes, but in one case took a little over 25 minutes. [7]

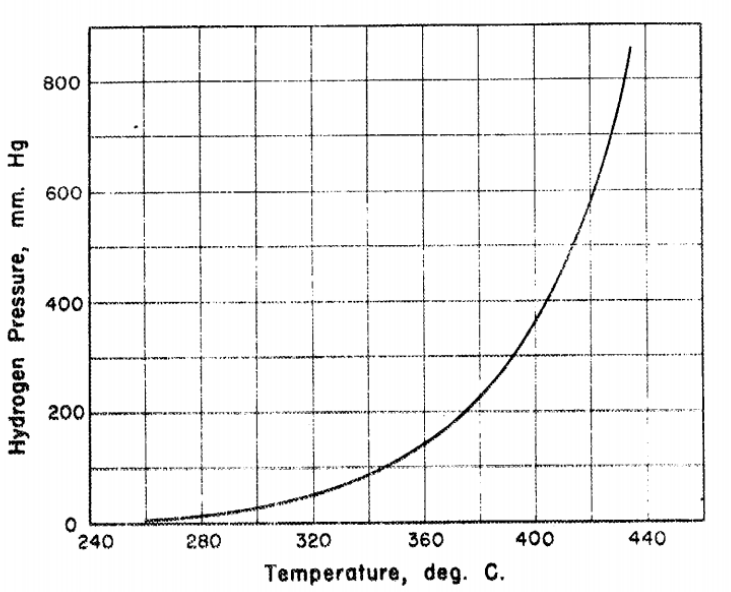

Figure 4. Pressure vs. temperature of dissociation for the dehydride reaction. [2]

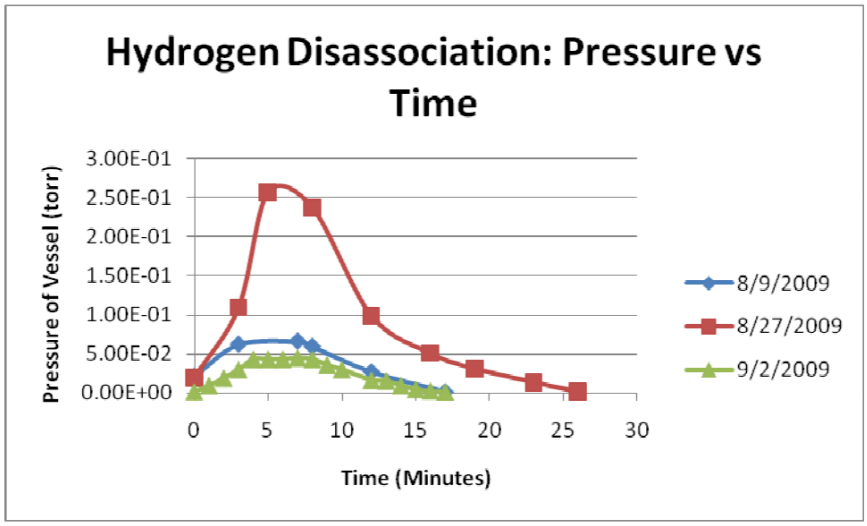

Fig. 4-13 Pressure vs Time during the dehyride step

Figure 5. The time scale of dehydride under varying vacuum pressures and the pressure increase associated with the release in hydrogen gas. [7]

Description of uranium powder

The powder that is produced is of interest because its properties will affect the quality of the pellets that are produced from it. Full powderization of uranium metal pieces is desired, and the size distribution of particles is of particular interest. Previous work by Bloch and by Condon found particle sizes to be ~40 μm. [5,8] In the process of interest uranium powder is pressed using a hydraulic or extrusion. Work by Helmreich has been performed that demonstrated these capabilities. [1]

The powder that was produced in this experiment was analyzed in an Argon atmosphere so as to obtain distributions for the metal powder, and not an oxide powder. In order to accomplish this, an Atmosphere Containment Vessel (ACV) was developed using fittings designed for glovebox use. An o-ring and clamp system allowed for powder to be placed in sample trays and sealed in with an Argon environment. The ACV is built on a 1.8 (0.75 in) cm tall, 6.35 cm (2.5 in) diameter nipple. A quartz, optical viewing port was selected to allow for optimal transmission of the visible light spectrum (>93%). The ACV is shown is Figure 6. The powder was analyzed a HIROX MX-5040SZ optical microscope. The microscope used allowed for resolutions of up to 800x and is shown in Figure 7.

Figure 6. The ACV with an alternate nipple size for viewing larger samples.

Figure 7. HIROX digital microscope used for powder imaging.

Description of process and facilities used

Uranium metal slugs were obtained from the Y-12 plant at Oak Ridge National Laboratory (ORNL) for use in this project as a part of the Nuclear Energy Research Initiative (NERI), under the Advanced Fuel Cycle Initiative (AFCI). These slugs are shown in Figure 8. They are stored in air, and have an oxide layer present on the surface. For the experiments performed in this work, these slugs were cutting using the diamond saw in Figure 9. The resulting cut samples are shown in Figure 10. After samples were cut, they were cleaned using an ultrasonic cleaner.

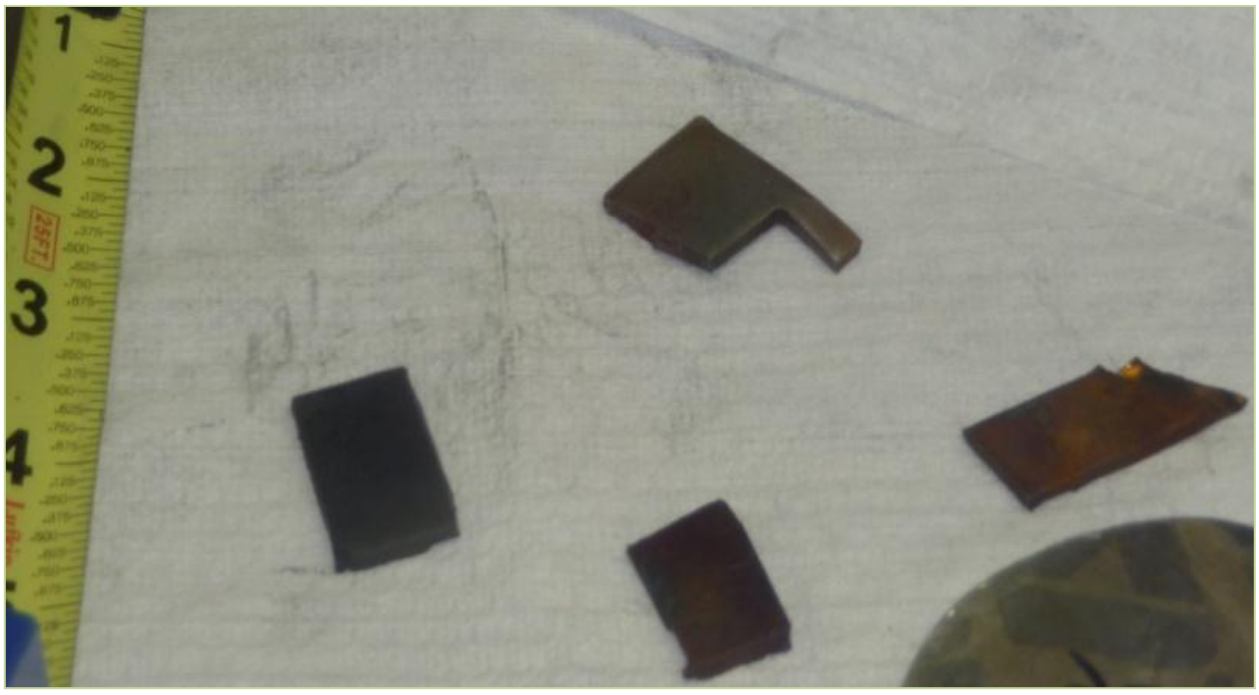

Figure 8. Uranium metal slugs from Y-12 in at ORNL. [7]

Figure 9. Diamond saw used for cutting uranium metal slugs into smaller sample sizes.

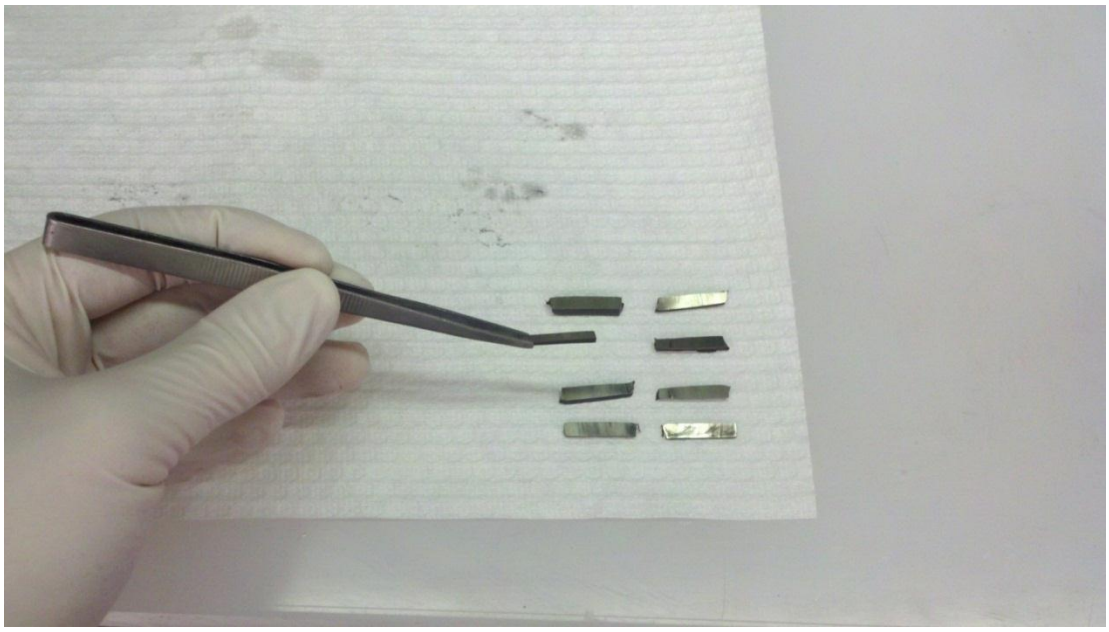

Figure 10. Cut uranium metal samples after being cut with the diamond saw and cleaned using an ultrasonic cleaner.

In order for the hydride reaction to proceed, the oxide layer must be removed from the uranium slugs. This is done by using a nitric acid wash, which removes the oxide layer based on Eq. 2. [9] The nitric acid used is a 35% by volume solution with water. The nitric acid process is conducted over ~10 minutes, and the uranium is removed once the oxide layer has been removed. If the uranium metal is left too long in the nitric acid solution, the nitric acid will begin to react with the uranium metal itself. This process is performed in an Argon atmosphere glovebag, shown in Figure 11. The uranium metal slugs were rinsed with deionized water after the nitric acid wash, let dry, rinsed with ethanol, and then let dry a second time. The ethanol rinse is to clean the surface and is conducted in a separate tray from the nitric acid as a safety precaution to prevent nitric acid-ethanol reaction.

$$UO_2 + 4HNO_3 \rightarrow U^{+4} + 2H_2O + 4NO_3^- \quad (2)$$

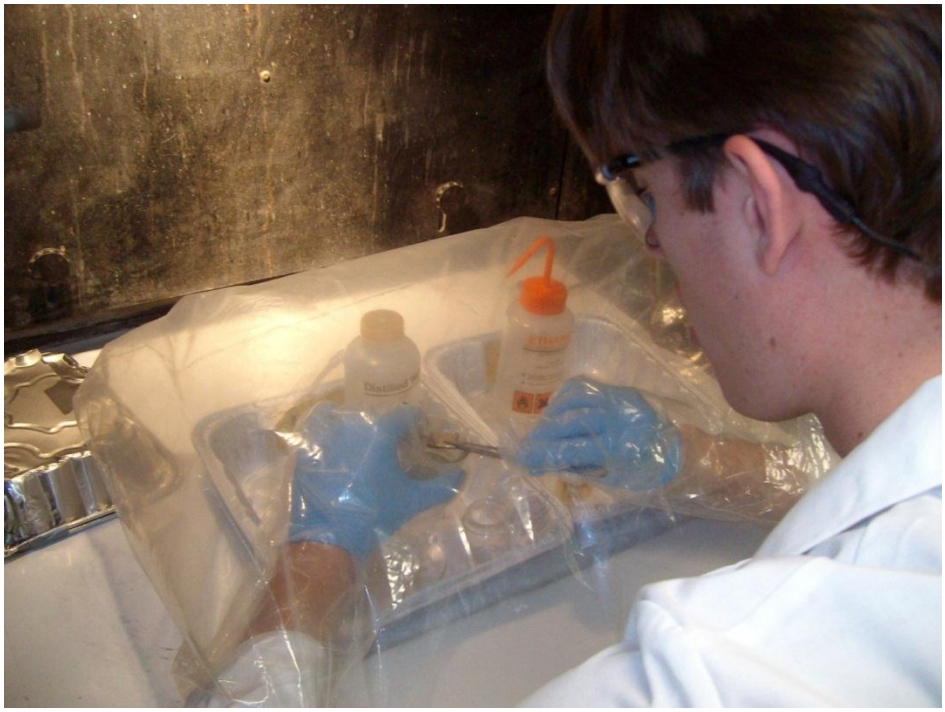

Figure 11. Acid wash station located inside a glovebag under argon atmosphere to reduce sample oxidation.

After the acid wash, the uranium slugs were transported to the glovebox in an argon filled container. The slugs were then used to make hydride-dehydride powder production runs.

The hydride-dehydride process used in this investigation was designed and developed by David J. Garnetti. [7] The reaction is contained within an aluminum-oxide crucible, held in a rig at the bottom of a furnace well as shown in Figure 12. The outside of the furnace system and furnace controls are shown in Figure 13. The whole system is held within an

Argon atmosphere glovebox, shown in operation in Figure 14. Preliminary experiments by Helmreich found that the reaction vessel used is capable of producing ~50 grams of powder in a 24 hour period, with approximately 50% conversion efficiency. The conversion efficiency of the reaction vessel has since been demonstrated to fully convert uranium metal to uranium metal powder.

Figure 12. Aluminum oxide crucible located at the bottom of the hydride-dehydride rig.

Figure 13. Furnace and furnace controls used in hydride-dehydride process.

Figure 14. Glovebox in operation, working at the hydride-dehydride station.

The aluminum-oxide reaction vessel is subjected to temperatures ~225°C and an argon-5%-hydrogen gas mixture for the hydride reaction. Gas flow to the furnace reaction chamber is cut off, a vacuum of 0.1 Pa (1E-3 Torr) is pulled on the chamber, and the furnace temperature is increased to temperatures around 325°C to dehydride the powder. For the reaction rate studies performed in this work, the mass of the sample was measured before the reaction and after completion. The mass of the remaining uranium metal slug was measured, as was the mass of the remaining slug and powder. This allowed for a determination if the powder was fully dehydrided. For both the hydride and dehydride reactions, the dwell time on the furnace was set. This means that the time of reaction was actually the measured time (dwell time) and the time required to heat up to the dwell temperature set (the temperature reported for each run).

Powder production runs were made to study the distribution of particle sizes and the hydride reaction rate. The hydride reaction rate was study with respect to temperature, gas pressure, and surface area. The dehydride reaction rate was not studied, and the same times and temperatures of dehydride were used for all experimental runs. This choice was made, as the dehydride reaction occurs over a much quicker timescale, and has little effect of the amount of powder produced. The dehydride reaction parameter of interest is the timescale required to fully dehydride the uranium-hydride powder produced.

CHAPTER II

PREVIOUS WORK AND MODELS

Thermal properties

The pressure dependent heats of formation of uranium hydride were calculated by Abraham and are given in Figure 15. [10]

Condon reported models for calculating the Gibbs' free energy and the standard enthalpy of formation for uranium-hydride as shown in Figure 16. Rate constant dependence on surface area, position on phase diagram, thermal history and other variables prevented Condon from fully characterizing these values. [11]

HEATS OF FORMATION OF UH_3, UD_3 AND UT_3 AT 25°

Expt. no.	$-\Delta H_f$ (cal./mole) UH_3	UD_3	UT_3
1	30,346	31,014	31,170
2	30,362	31,039	31,114
3	30,347	31,011	31,140
Mean	30,352	31,021	31,141
Est. error	±30	±30	±50

Figure 15. Heats of formation of uranium hydride. [10]

$$\Delta G_f^\circ(\mathrm{UH_3}, T)/\mathrm{J\ mol^{-1}} = 720.7(T/\mathrm{K}) - 182.6 \times 10^{-3} - 70.34(T/\mathrm{K})\ln(T/\mathrm{K}),$$
$$\sigma/\mathrm{J\ mol^{-1}} = 0.26(T/\mathrm{K}) \approx 180,$$
$$\Delta H_f^\circ(\mathrm{UH_3}, T)/\mathrm{J\ mol^{-1}} = 182.6 \times 10^3 + 70.34(T/\mathrm{K}), \qquad \sigma/\mathrm{J\ mol^{-1}} = 117 \text{ to } 620,$$
and
$$\Delta C_p^\circ/\mathrm{J\ K^{-1}\ mol^{-1}} = 70{,}37, \qquad \sigma/\mathrm{J\ K^{-1}\ mol^{-1}} = 5.6.$$

Figure 16. Models developed by Condon for the Gibbs' free energy and the standard enthalpy of formation for uranium-hydride. [11]

Albrecht and Mallett

The primary result of work by Albrecht was the formation of linear rate Eq. 3,

$$r = 4.11 * 10^{-3} p^{\frac{3}{4}} \exp\left(-\frac{1820}{RT}\right) \tag{3}$$

where r is the linear rate in ml/cm^2*sec, p is in mm Hg, R is the gas constant in cal/K*mol, and T is temperature in K. Eq. 3 is valid for temperatures from 96-250°C. Albrecht also notes variations on Eq. 3 with temperature and pressure. [12]

Bloch

Work by Bloch focused on the development of linear reaction rate constants for the uranium-hydride reaction. [5] The linear kinetic constant, k_L is defined as Eq. 4,

$$k_L = \frac{d\alpha(t)}{dt} \tag{4}$$

where $\alpha(t)$ is the time dependent reaction and t is time. [5] The temperature and pressure dependence of the linear kinetic constant are addressed in Eq. 5,

$$k_L(P,T) = k_{L0}(T)\left(\frac{P}{P_0} - 1\right)^2 \quad (5)$$

where P is the hydrogen pressure, P_0 is the absorption equilibrium pressure, T is temperature, and k_{L0} is the pressure-independent linear rate constant. Bloch quantified the temperature dependence of $k_{L0}(t)$ in Figure 17. Bloch quantified the quadratic relationship between the rate constant and pressure in Figure 18. [5] This work by Bloch forms a strong basis for ideal, lab scale experiments.

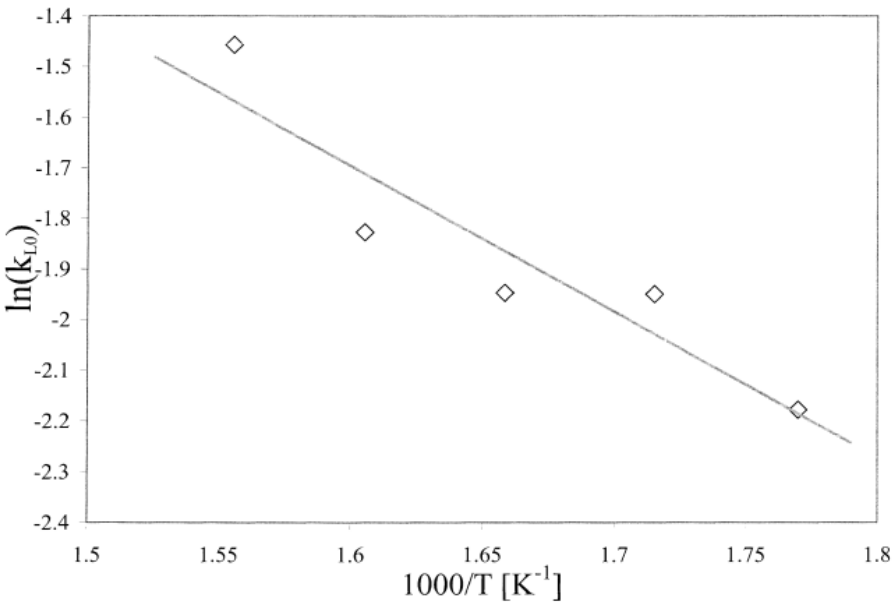

Figure 17. Temperature dependence of the pressure-independent linear rate constant. [5]

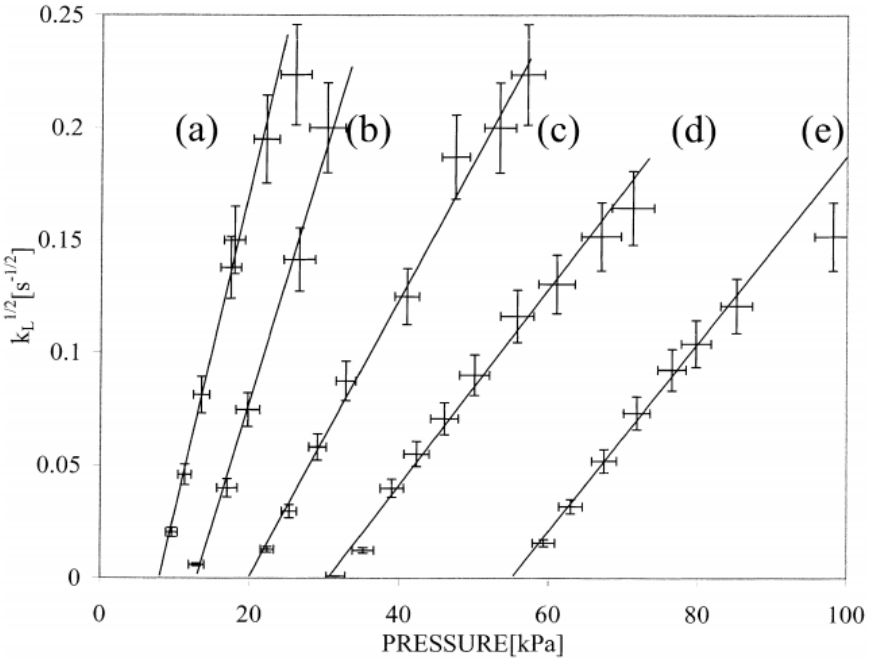

Figure 18. Pressure dependence of the square root of the linear hydriding rate constant for (a) 294°C, (b) 313°C, (c) 332°C, (d) 352°C, and (e) 371 °C. [5]

Condon

Work by Condon was done to quantify the diffusion of hydrogen into a uranium sample. This work was based on the diffusion Eq. 6,

$$D\frac{\partial^2 C}{\partial x^2} = \frac{\partial C}{\partial t} - a\frac{\partial U}{\partial t} \tag{6}$$

where D is the diffusion coefficient, C is the atomic concentration (in mole fraction) of hydrogen, U is uranium content expressed as a mole fraction, t is time, and a is the stoichiometric ratio for the reaction (=3). [13] Further definition is given in Eq. 7,

$$-\frac{\partial U}{\partial t} = k_1 C U \tag{7}$$

where k_1 is the rate constant. [13] The following values are defined as a function of Temperature:

$$k_1 = 10.4 * \exp\left(\frac{1592}{T}\right) \sec^{-1} * (mole\ fraction\ of\ H)^{-1} \tag{8}$$

$$D = 1.9 * 10^{-6} \exp\left(-\frac{5820}{T}\right) \tag{9}$$

where D is in units of m^2/sec and T is the temperature in K. [13] The initial atomic concentration is set as a boundary condition for the solution and is given by

$$C_0 = 5.58 * 10^{-4} \exp\left(-\frac{894}{T}\right) P^{\frac{1}{2}} * (mole\ fraction\ of\ H) \tag{10}$$

where P is pressure in Pa. This model is then further explored, and the proposed inclusion of a constant for dehydriding is discussed. This is a useful model for determining the depth of penetration and the reaction fraction as a function of depth. [13]

CHAPTER III

RESULTS

Powder characterization

The powder produced in a preliminary run was analyzed using ImageJ (version 1.38x 2007) image analysis software. The software allowed for gray scale image analysis and the calculation of particle size distributions by determining the number of pixels in each particle, and relating that to the scale of the image taken. Spherical particles were assumed, and reported values are given in terms of calculated diameter and spherical volume. Particle boundaries were identified, and analysis was carried out on a 5895 particle set. The results of this run are shown in Figure 19 and an example of a characteristic powder image at 800x is shown in Figure 20. [14] The main contribution to the volume of the powder sample was of particles in the 25-78 μm range, with a peak ~44 μm. These results fit with previous experiments by Bloch and Condon which found the characteristic size ~40 μm. [5,8]

Run #1 (as detailed in the Appendix) was conducted and shown to have particles within the same order of magnitude as the previous run. An image of this run is shown in Figure 21. After this, further particle distribution analysis was concluded.

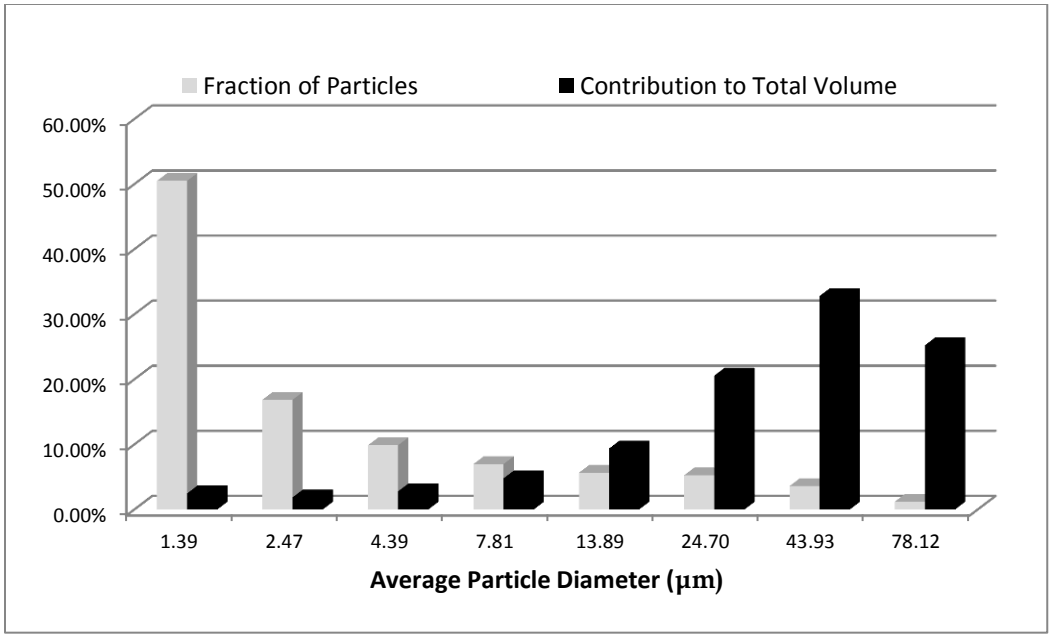

Figure 19. Results from image analysis of a preliminary run. [14]

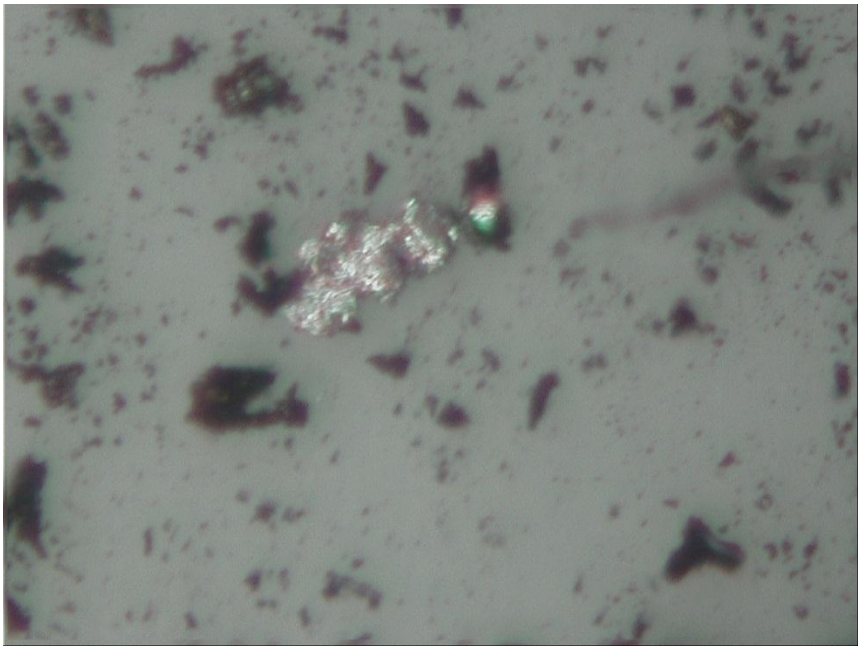

Figure 20. Image of powder from preliminary calculations at 800x.

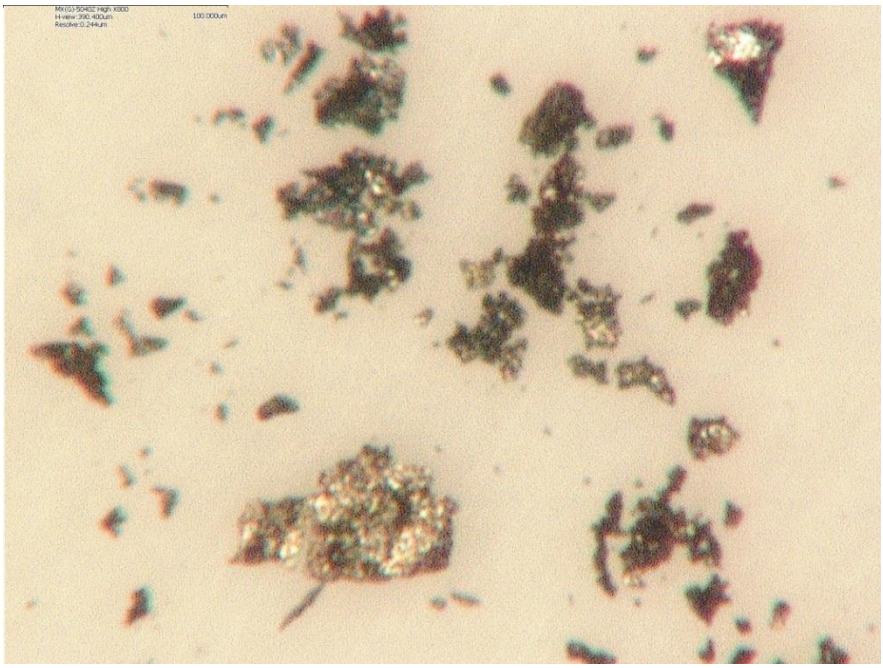

Figure 21. Image of powder from Run #1 at 800x.

Reaction dependence studies

The rate of reaction was determined by holding system pressure constant at 5 psig, hydride temperature constant at 250°C, and dehydride temperature at 325°C. Other variables held constant are given in the Appendix A. An S-curve shape appears, as expected based on previous work. [5] The S-curve shape of the data occurs due to an initial lag in reaction rate due to breakdown of the initial oxide layer and a relatively smooth initial reaction surface. The reaction speeds up due to increases in reaction surface area, but eventually slows down as the amount of uranium metal to react

becomes smaller than the amount of powder produced. The Avrami Equation can be used to model such a reaction. The Avrami Equation is given by

$$\alpha = 1 - \exp(-kt^n) \quad (11)$$

where α is the reaction fraction (powder yield), t is time in seconds, and k and n are constants. When ln(ln(1/(1- α))) is plotted versus ln(t), the slope is the constant n and the intercept is ln(k). These values are plotted in Figure 22 for the uranium hydride reaction rate as calculated from the data in Appendix B. The Avrami Equation constants were found to be k= 3.783E-6 and n=2.1294. The experimental data from Appendix B and the fitted Avrami Equation are plotted in Figure 23.

The Avrami Equation approaches complete powderization as time approaches infinity. To reach 99% powderization, a time of 562 minutes is required. This value, an approximate time for most of the powder to react, should only be used for only small changes in system parameters, but as long as the same pressure and temperatures are used, it may be scalable (depending on the result of future surface area calculations).

The reaction characteristics with respect to temperature were studied for runs at 5 psig, 270 minute hydride, and 325°C dehydride. The data was graphed and fit with an exponential curve as shown in Figure 24. The fit resulted in Eq. 12,

$$\alpha(T) = -0.00077631 * T^2 + 0.78654162 * T - 198.68740459 \quad (12)$$

where α is the reaction fraction (powder yield) and T is temperature in Kelvin. This parabolic relationship with temperature was demonstrated previously by Bloch. [5] Eq. 12 should be only be used for temperatures close to the range of temperatures used to calculate it and care should be given to the extrapolation of this equation to other pressures. The derivative of Eq. 12 was set equal to zero to determine the maximum. The maximum powder yield occurred at a temperature of 233°C.

The reaction characteristics with respect to pressure were studied for runs at 270 minute hydride, 250°C hydride, and 325°C dehydride. The data was graphed and fit with an exponential curve as shown in Figure 25. The fit resulted in Eq. 13,

$$\alpha(P) = -0.00437970 * P^2 + 0.08883989 * P - 0.01002987 \qquad (13)$$

where α is the reaction fraction (powder yield) and P is pressure in psig. This gauge pressure is the pressure resulting from the argon-5%-hydrogen gas flowing through the reaction chamber. Previous work has supported the modeling of pressure dependence based on fractional exponents. [10,12] The quadratic relationship was used to fit the data due to its good fit and based on the presumption that at some point additional gas pressure could impede the reaction. More data at higher pressures is needed to better determine the behavior of this pressure dependence.

Data was collected to determine the effect of surface area on the reaction. The data is presented in Figure 26. The surface area was calculated by adding the area of all but one side of the cut metal slug, which approximates a rectangle. One of the bottom sides was not included, as the sample was set on this side in the aluminum oxide crucible. This blocked the reaction area of that side. The blocked side was always one of the largest surface area sides (dimension y by dimension z in the Appendix). More data needs to be collected with respect to surface area to try and find a correlation. The data presented here does not appear to show a correlation, but errors in measurement could account for this.

The powder yield in each run was measured after a dehydride reaction was run on the hydride powder. The dehydride reaction was run for 20 minutes of dwell time.

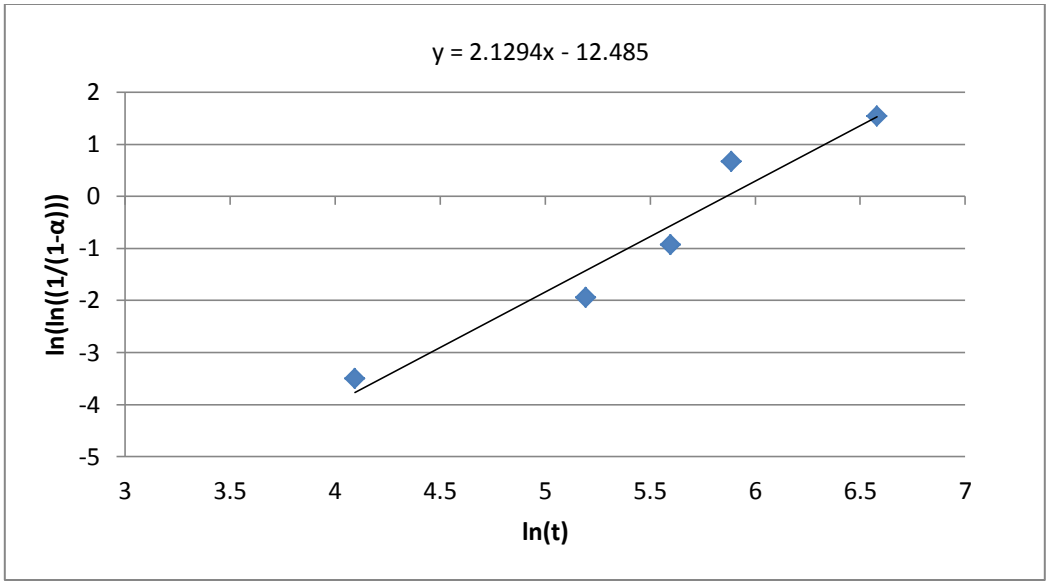

Figure 22. ln(ln(1/(1- α))) vs. ln(t) for runs at 5 psig, 250°C hydride, 325°C dehydride used for calculation of the parameters k and n for the Avrami Equation.

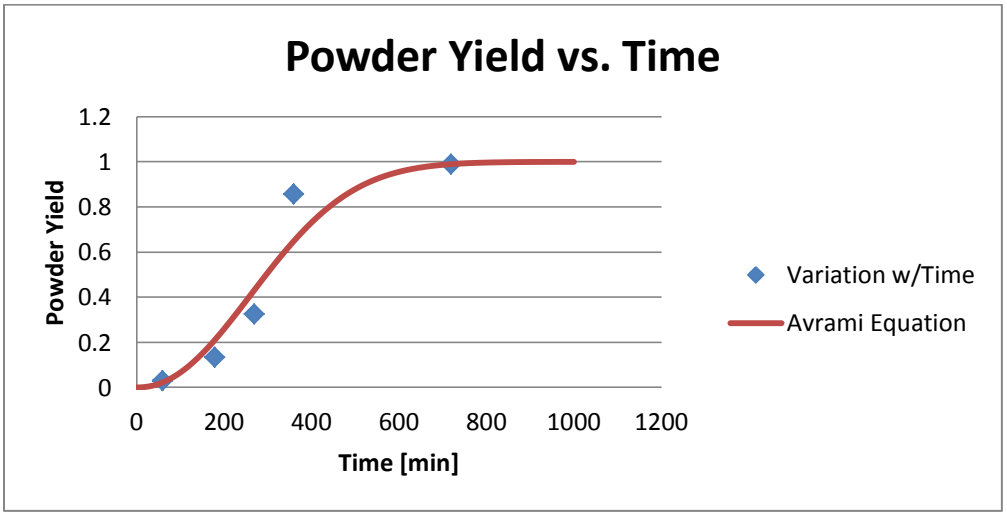

Figure 23. Powder yield vs. dwell time for runs at 5 psig, 250°C hydride, 325°C dehydride.

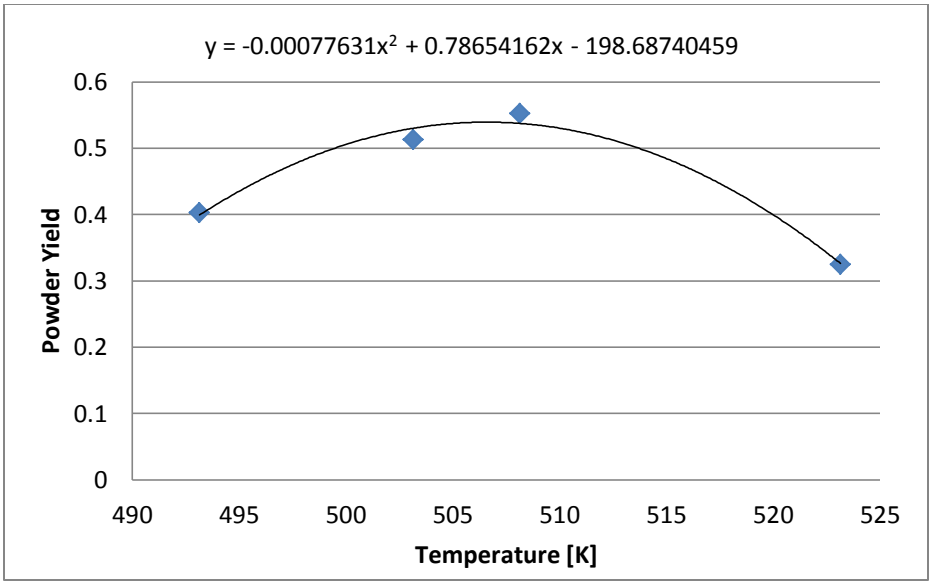

Figure 24. Powder yield vs. temperature for runs at 5 psig, 270 minutes, 325°C dehydride.

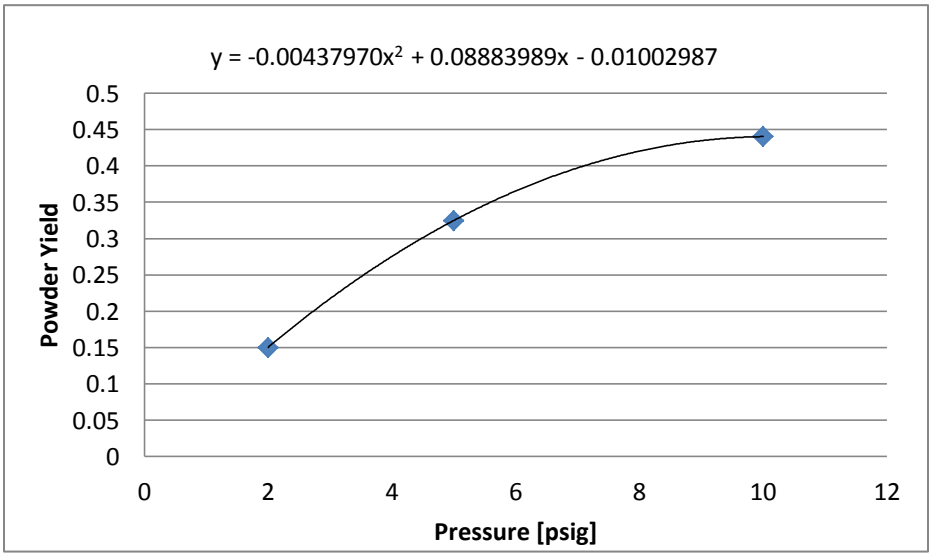

Figure 25. Powder yield vs. pressure for runs at 270 minutes, 250°C hydride, 325°C dehydride.

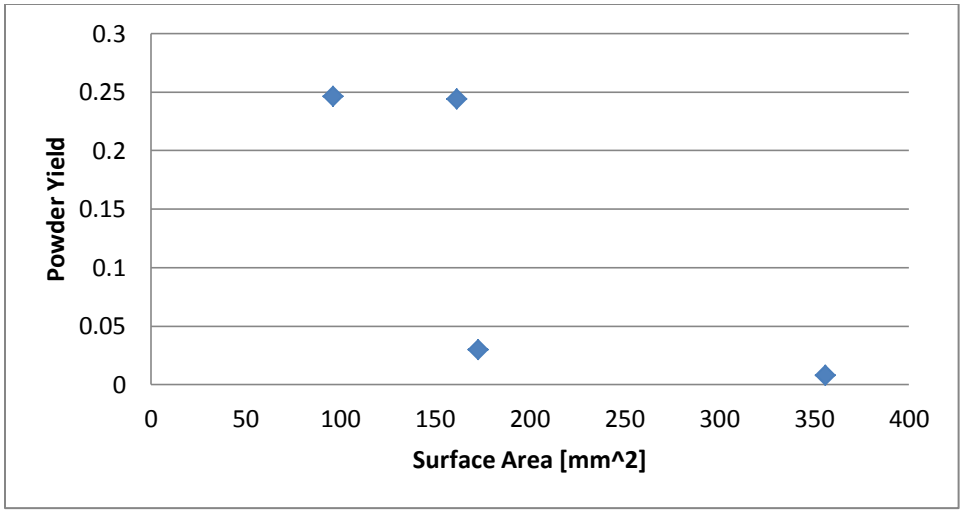

Figure 26. Powder yield vs. surface area for runs at 60 minutes, 5psig, 250°C hydride, 325°C dehydride.

Sources of error

Several practicalities of experiment operation may have introduced error or uncertainties into this analysis. The time required to heat each sample up to the desired hydride temperature would vary between different temperatures and contribute to error in comparing temperature runs where time was meant to be held constant. The process of separating the unreacted metal slug from the uranium powder produced may have led to small losses of powder before mass measurement. Incomplete dehydriding of reacted powder may have added mass to some of the reported final masses. Of the potential sources of error, accounting for the start-up heat transient could be accounted for with a different measurement of reaction time. Incomplete dehydride of reacted powder could be accounted for by dehydriding at a higher temperature, increasing the time of dehydride, or a combination of both.

CHAPTER IV

CONCLUSIONS

Process optimization

The reaction rate studies conducted of the hydride-dehydride process in use at Texas A&M in the FCML have produced the following recommendations for process optimization:

- Maximize the reaction vessel pressure
- Run the hydride process near 233 °C
- Run the dehydride process at a minimum of 325 °C under a vacuum of 0.1 Pa for at least 25 minutes. Higher temperatures can be used, but should remain below 400 °C in order to reduce sample self-sintering. [7]
- To ensure complete powderization, Eq. 11 or similarly derived equations should be used to determine the run time necessary. For the parameters used in this experiment, 562 minutes was calculated to produce complete powderization.

The laboratory scale process used in this work is not the most effective way of producing large amounts of uranium powder. For process commercialization, a different system should be used. In order to allow for process heating and maximization of reaction surface area a rotary kiln would be an efficient system for powder production.

A rotary kiln is a kiln that spins during operation. The spinning action is desired to separate powder from the surface of uranium slugs, which allows for continued reaction of the uranium slug to form uranium-hydride powder. A rotary kiln designed at ORNL for the powderization of uranium dioxide using voloxidation is shown in Figure 27. Voloxidation powderizes used nuclear fuel (UO_2 + fission products) by reacting UO_2 with O_2 at increased temperatures. This rotary kiln was still considered laboratory scale, as it could handle a limit of 20 kg of processing per year. The design allowed for single pass or recirculation of gas flow, rotational speeds up to 10 RPM, and an operational temperature range of 200-600°C. [15]

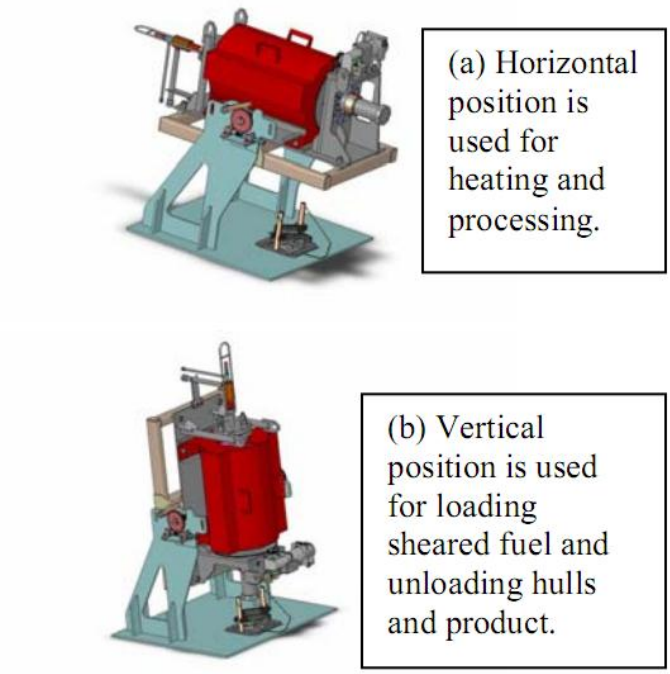

Figure 27. Rotary kiln designed at ORNL for use in voloxidation. [15]

Optimal design characteristics for a commercial scale hydride process:

- Gas recirculation
- Ability to use same vessel for hydride and dehydride process
- Inert operation environment
- Furnace capabilities up to at least 400 °C
- Ability to draw a vacuum on the system
- Method for removal of powder layer from metal slugs (rotary kiln suggested)

Future work

Work still needs to be done to relate the microscopic models developed by previous work to macroscopic models published in this work. The diffusion model of Condon, the linear kinetic constants of Bloch, and the work of others present a wealth of knowledge on this process, but appear to be limited to lab scale experiments. While the work published here was done for small sample sizes, it represents progress towards macroscopic system quantification oriented at system optimization.

REFERENCES

[1] G.W. Helmreich, M.S. thesis, Texas A&M University (2010).

[2] P. Chiotti and B.A. Rogers, United States Atomic Energy Commission, AECD-2974 (1950).

[3] J. Bloch and M.H. Mintz, International Atomic Energy Commission (IAEC) Annual Report (2001) 53-75.

[4] J.F. Bingert, R.J. Hanrahan Jr., R.D. Field, and P.O. Dickerson, J. Alloys and Compounds 365 (2004) 138-148.

[5] J. Bloch, Journal of Alloys and Compounds 361 (2003) 130–137.

[6] J.B. Condon, J. Less-Common Met. 73 (1980) 105.

[7] D. J. Garnetti, M.S. thesis, Texas A&M University (2009).

[8] J.B. Condon, E.A. Larson, J. Chem. Physics, 59 (2) (1973) 855-865.

[9] G.W. Helmreich, Verbal Description of Nitric Acid Chemistry (2011).

[10] B.M. Abraham and H.E. Flotow. J. Am. Chem. Soc. 77 (6) (1955) 1446–1448.

[11] J.B. Condon, J. Chem. Thermodynamics (1980) 1069-1078.

[12] W.M. Albrecht and M.W. Mallet, J. Electrochemical Society, 103(7) (1955) 404-409.

[13] J.B. Condon, J. Phys. Chem. 79 (1975) 392.

[14] G.W. Helmreich, W.J. Sames, D.J. Garnetti, and S.M. McDeavitt, Trans. of the Am. Nuclear Society, 102 (2010).

[15] B. B. Spencer, G. D. Del Cul, E. C. Bradley, R. T. Jubin, T. D. Hylton, and E. D. Collins, Trans. of the Am. Nuclear Society, 98 (2008) 103-104.

APPENDIX A

EXPERIMENTAL DATA

Run #	mass_start [g]	mass_slug_final [g]	mass_total_final [g]	Overall Mass Change [g]	mass_powder [g]	Yield of Powder [mass of powder/mass initial]	P [psi]	Flow Rate [scfh]	T_hydride [°C]	T_dehydride [°C]	t_hydride [min]	t_dehydride [min]	Dimension x [mm]	Dimension y [mm]	Dimension z [mm]	Surface Area [mm^2]
1	1.5384	1.3082	1.513	-0.0254	0.2048	0.13312533	5	3	250	325	180	20	1.62	3.57	15.93	120.0501
2	1.436	0.1973	1.4272	-0.0088	1.2299	0.85647632	5.4	3	250	325	360	20	1.61	3.57	15.89	119.3885
3	1.5222	1.4767	1.5219	-0.0003	0.0452	0.02969386	5.2	3	250	325	60	20	1.46	3.6	16.03	115.0276
4	1.3761	0	1.3629	-0.0132	1.3629	0.99040767	5	3.3	250	325	720	20	1.32	3.61	15.82	108.4054
5	1.2757	1.0101	1.3214	0.0457	0.3113	0.24402289	5	3	250	325	60	20	1.11	3.62	16.22	102.7612
6	1.4017	1.0113	1.4664	0.0647	0.4551	0.32467718	5	3	250	325	270	20	1.34	3.62	15.95	110.1866
7	1.3802	0.703	1.4659	0.0857	0.7629	0.55274598	5	3	235	325	270	20	1.33	3.57	15.87	108.3663
8	1.3785	0.8929	1.4485	0.07	0.5556	0.40304679	5	3	220	325	270	20	1.35	3.53	16.08	109.7094
9	0.04062	0.4003	0.4103	0.36968	0.01	0.24618415	5	3	250	325	60	20	0.86	3.5	10.34	59.9948
10	2.4785	2.1538	2.5259	0.0474	0.3721	0.15013113	2	3	250	325	270	20	1.99	3.54	18.82	155.6156
11	5.4344	5.403	5.4454	0.011	0.0424	0.00780215	5	3.1	250	325	60	20	3.84	4.24	20.02	271.2016
12	1.7569	0.941	1.8427	0.0858	0.9017	0.51323354	5	3	230	325	270	20	1.28	3.78	19.05	130.4538
13	1.953	1.1414	2.0015	0.0485	0.8601	0.44039939	10	3	250	325	270	20	1.45	3.78	19.59	141.8232

APPENDIX B

DATA FOR CALCULATION OF AVRAMI EQUATION

CONSTANTS

t [min]	α	ln(t)	lnln(1/(1- α))
60	0.029694	4.094345	-3.50178
180	0.133125	5.192957	-1.94588
270	0.324677	5.598422	-0.93505
360	0.856476	5.886104	0.663335
720	0.990408	6.579251	1.536177

CONTACT INFORMATION

Name:	William James Sames V
Professional Address:	c/o Dr. Sean McDeavitt Department of Nuclear Engineering MS 3133 Texas A&M University College Station, TX 77843
Email Address:	will.sames@gmail.com
Education:	B.S., Nuclear Engineering, Texas A&M University, May 2011 Latin Honors Honors Undergraduate Research Fellow University Honors Foundation Honors Engineering Scholars Program Alpha Nu Sigma